Pad Force Required in Shear-deformation Sheet Forming of Curved Hat Channels for Ultra-High-Strength Steels

Saaya Kanayama[1*], *Tohru* Yonebayashi[1], *Yasuharu* Tanaka[2], and *Shunji* Hiwatashi[3]

[1]Nippon Steel Corporation, Research & Development, 1-8 Fuso-Cho, Amagasaki, Hyogo, 660-0891, Japan
[2]Nippon Steel Corporation, Nagoya Works, 5-3 Tokai-machi, Tokai, Aichi, 476-8686, Japan
[3]Nippon Steel Corporation, Research & Development, 20-1 Shintomi, Futtsu, Chiba, 293-8511, Japan

Abstract. One of the latest challenges in sheet forming of crashworthy lightweight automotive parts is the cold stamping of curved hat channels. Neither cracking in convex bottom nor wrinkling in concave bottom can be avoided in conventional drawing. Tanaka and others have proposed in-plane shear forming technology, in which shear strains are given to vertical walls by pad draw-bending for the case of curved channels. This requires a sufficient pad force to clamp the bottom face area; however, the minimum pad force for successful forming can be known only by trial and error. In this study, we focused on cracking in convex bottom and examined a method to estimate the required pad force. Finite element simulations and forming experiments for a 980-MPa-grade steel led to a theoretical model in which three types of force were applied to the flat bottom during forming: a force given by in-plane shear of walls, a frictional force given by the pad force for clamping, and a resistance against the flow to the convex bottom. The required pad force could then be obtained as a solution of the equilibrium of these forces. Furthermore, the validity of the proposed method was confirmed.

Keywords: Production manufacture; Forming process; Ultra-high-strength steel; Sheet forming.

1 Introduction

High-strength steel sheets with a tensile strength of 980 MPa or higher have been widely used for body parts of automobiles to achieve both crashworthiness and lightweight. However, the higher the strength of the steel, the lower its elongation, making cold stamping of complex shapes, such as longitudinally curved hat channels, and T-shape parts, more difficult. Tanaka's group has proposed in-plane shear forming technology, which can avoid both thinning in tension and wrinkling in compression by using in-plane shear deformation without thickness changes. They applied draw-bending to such curved channels [1], and experimentally validated that even 1470-MPa-grade steel was applicable to the rear part of a front-side member, with a 3-dimentionally curved shape, by using the in-plane shear draw-bending [2].

Fig. 1 shows a schematic of the in-plane shear draw-bending and Fig. 2 shows the die set structure of that for an S-shaped hat channel. In conventional drawing shown in Fig. 1(a), the material in the walls flows perpendicularly to the blank-holder face, which causes the material flow from the convex area to the concave area of the bottom. This causes cracking in convex bottom and wrinkling in concave bottom. In contrast, in the in-plane shear draw-bending, the blank is draw-bent as shown in Fig. 1(b) by using the die set shown in Fig. 2, where the flanges are clamped between a blank-holder and a die, and the bottom is clamped between a pad and a punch. Consequently, the material flow of the bottom is suppressed, and in-plane shear is achieved in the walls. This suppresses the cracking and wrinkling.

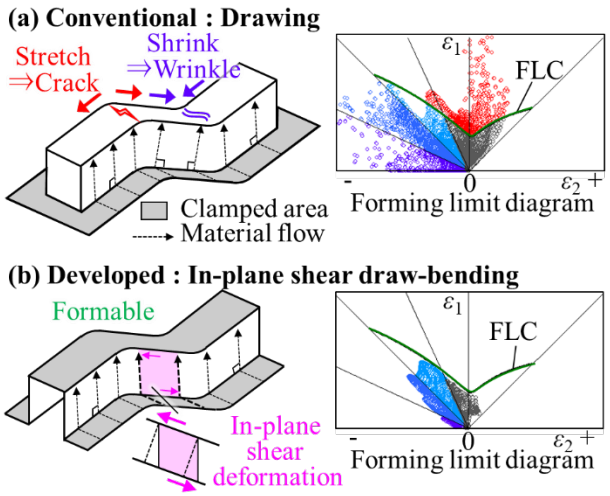

Fig. 1. Schematic diagram of in-plane shear forming [1,2]

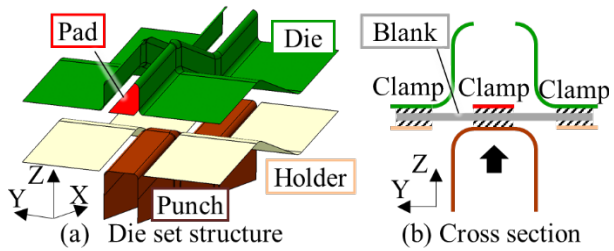

Fig. 2. Die set structure of in-plane shear forming

* Corresponding author: kanayama.74r.saaya@jp.nipponsteel.com

However, this forming requires a large pad force, and an insufficient pad force causes in cracking and wrinkling similar to those in conventional drawing (Fig. 3). Smaller pad force is ideal for reducing the burden on the die set; hence, a quantitative estimation of the minimum pad force required for successful forming is desired. However, finding the required pad force still depend on trial and error, and, thus, a method for estimating this value is required.

In this study, we focused on cracking in convex bottom, and developed the method for estimating the required pad force using finite element (FE) analyses and press experiments.

Fig. 3. Example of cracking and wrinkling owing to insufficient pad force

2 Methods and procedures

The shapes investigated were convexly curved in the longitudinal direction at various slope angles and had a hat-shaped cross section with constant height, as shown in Fig. 4. FE simulations and press experiments for them were performed to confirm the formability in in-plane shear draw-bending. The material is a sheet steel with a thickness of 1.4 mm and a strength grade of 980 MPa.

Slope angles θ of 10° and 20° were chosen for FE simulations. The blank holding force was set to 147 kN and pad force were changed from 98 to 294 kN. LS-Dyna Ver. 971, which is a general-purpose dynamic explicit solver, was used. The element type was a square shell element with an element size of 1-mm. The number of integration points in the thickness direction was set to 7, and the friction coefficient was set to 0.10. The Hill '48 yield function with an isotropic in-plane r-value was used for the material model. The work hardening was approximated by the Swift hardening law of which parameters identified by tensile tests are shown in Table 1. A thickness reduction of 20% was assumed as the forming limit for cracking.

The press forming experiments were performed for a shape with $\theta = 20°$. The other conditions were the same as those in the FE simulations. The optical strain evaluation system (ARGUS, manufactured by GOM of Germany) interpreting dot marks originally painted of blank sheets at 1-mm interval was used to evaluate the strains in a press-formed part.

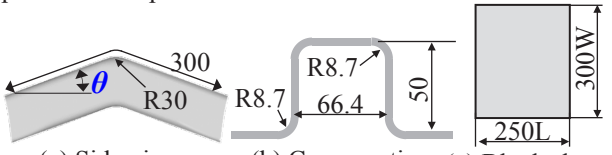

Fig. 4. Model part shapes and blank shape

Table 1. Material parameters

K [MPa]	n	ε_0	$\bar{r}$
1300	0.07	0.0006	0.8

3 Results and discussion

3.1 Results of FE simulations

Fig. 5 shows the simulated thickness reduction for $\theta = 20°$. Decreases in the pad force caused increases in the thickness reduction at the flat end where the convex fillet starts in the bottom, and the reduction exceeding 20% at a pad force of 98 kN. Fig. 6 also shows the major and minor strains at the end of forming. At the flat end, plane strain stretching in the longitudinal direction occurred, and increasing slope angle θ and decreasing pad force enhance the stretching. The strain states in vertical walls were concentrated near pure shear, and the magnitude of strains increased as the slope angle θ increased. Furthermore, the wall strains for θ = 20° decreased with decreasing pad force, whereas the pad force had a minimal effect for θ = 10°. This is because, for an ideal state in which the wall material flows parallel to the press direction as shown in Fig. 1(b), the magnitude of the shear strains in the walls is determined by the part shape, particularly by the slope angle θ. The combination of a steep slope and a low pad force tends to keep away from the ideal state and, thus, increases the risk of cracking.

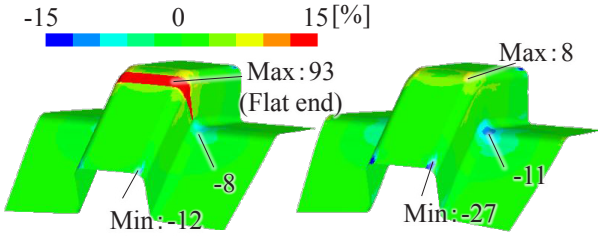

Fig. 5. Effect of pad force on sheet thickness reduction

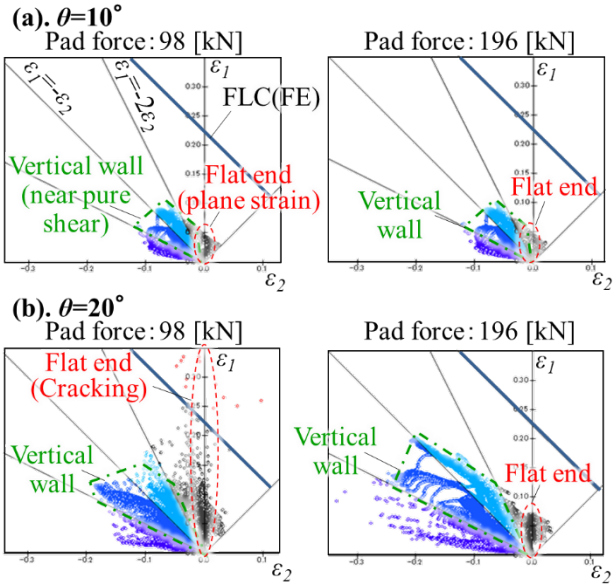

Fig. 6. Effect of θ and pad force on major and minor strains

3.2 Results of press experiments

Table 2 presents the experimental results. A pad force below 118 kN resulted in necking or cracking at the bottom flat end, and a pad force over 129 kN resulted in a successful forming. The required pad force is in between

118 and 129 kN, which is almost in accordance with the FE analyses. Fig. 7 shows the comparison of the maximum value of major strains at the bottom flat end between FE simulations and press experiments. The strains were close each other for successful cases, and, thus, the FE simulations could reproduce the press experiments.

Table 2. Experimental formability on pad force effect

Pad force [kN]					
78	88	118	129	137	193
Crack	Necking		Formable		

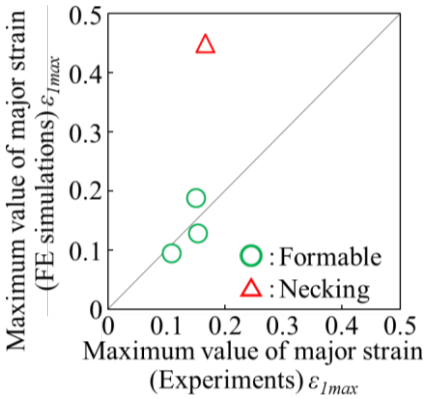

Fig. 7. Comparison of the maximum major strains at bottom flat end between FE simulations and press experiments

3.3 Theoretical model for deriving required pad force

As mentioned earlier, the longitudinal friction given by pad force is essential to cause appropriate in-plane shear in the walls in in-plane sear draw-bending [1]. Therefore, we constructed the following theoretical model for deriving the required pad force from the equilibrium condition of the longitudinal forces acting on the flat part of bottom during forming.

As shown in Fig. 8, there are three longitudinal forces acting on the flat bottom: a force on the edges BC and DA given by in-plane shear of walls (F_1), a frictional force on both sides of the area ABCD given by the pad force for clamping (F_2), and a resistance on the edge AB against the flow to the convex bottom (F_3). The equilibrium equation for the balance of these forces is as follows:

$$F_1=F_2+F_3 \tag{1}$$

Here, under the formable condition, F_3 cannot exceed the force at the forming limit of the material; hence, F_2 cannot be less than the difference between F_1 which depends on the part geometry and the maximum value of F_3 at forming limit. The required pad force F_p can then be calculated from the friction coefficient μ and this critical value of F_2.

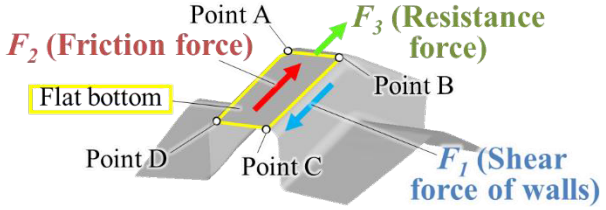

Fig. 8. Theoretical model of forces acting on the flat bottom

3.4 Verification of theoretical model by using FE simulations

Eq. (1) was verified using the results of the FE simulations. Fig. 9 shows the method of deriving F_1 and F_3. Both the experiment and simulations showed that cracks owing to insufficient pad force occurred in the early forming stages before 15-mm stroke. Furthermore, F_2 reached its maximum value at the stroke when the crack occurred in FE simulation. Therefore, our verification targeted the small forming stroke at which F_2 reached maximum.

Firstly, F_1 was derived using the following equation:

$$F_1=\frac{2Lt\sum\tau_1}{N} \tag{2}$$

where τ_i is the in-plane shear stress of each element along the edge BC or DA, N is the number of elements along that, L is the longitudinal length along that, and t is the thickness of the material.

F_2 was calculated by summing the longitudinal force acting on both sides of surface ABCD from the pad and the top surface of punch.

F_3 was derived using the longitudinal stress σ_{Li}, width W_i, and sheet thickness t_i in each element along the edge AB as follows:

$$F_3=\sum\sigma_{Li}t_iW_i \tag{3}$$

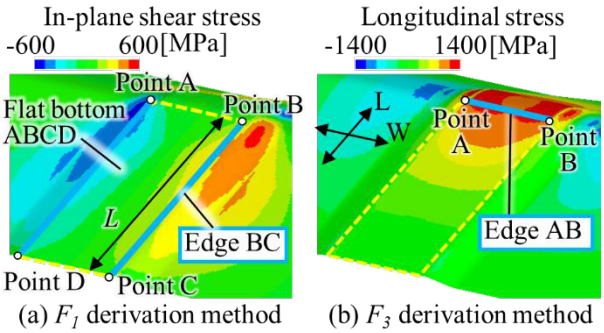

Fig. 9. F_1 and F_3 derivation methods

Fig. 10 shows the results of verifying the validity of Eq. (1). The left-hand side (F_1, vertical axis) and right-hand side (F_2+F_3, horizontal axis) of Eq. (1) were almost identical under all conditions, thereby demonstrating the validity of Eq. (1).

Fig. 11 shows the effect of the forming conditions on each force term in Eq. (1). First, F_1 increased mainly with increasing θ. This result was thought to be due to the wall deformation depending mainly on θ, as shown in Fig. 1(b). Next, F_2 mainly increased as the pad force increased. This result was thought to be due to the normal force acting from the pad and punch to the bottom mainly depending on the pad force. Finally, F_3 increased as θ increased, and as the pad force decreased. As shown in Eq. (1), F_3 was thought to change in accordance with the changes in the difference between F_1 and F_2.

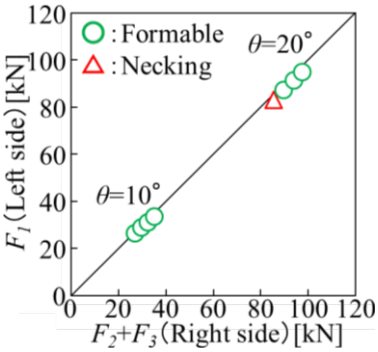

Fig. 10. Results of Eq. (1) verification

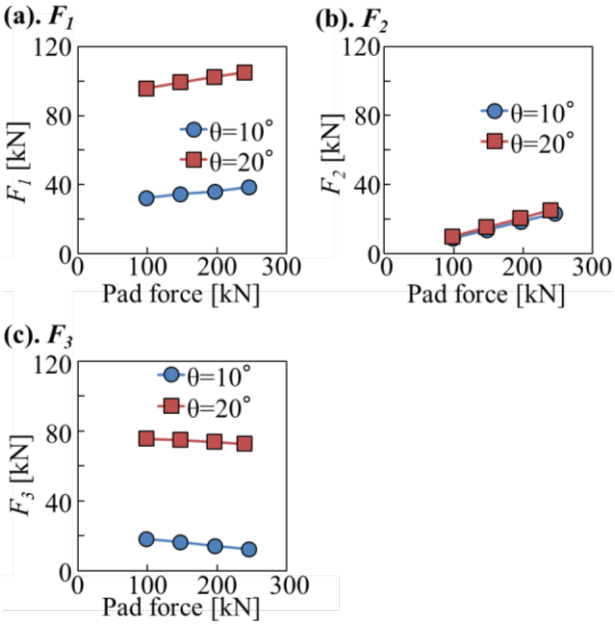

Fig. 11. Effect of θ and pad force on F_1, F_2 and F_3

3.5 Required pad force derivation method using theoretical model

We estimated from Fig. 2 that F_1 mainly depended on θ. Furthermore, F_3 was given by plane strain stretching at the flat end; hence, we assumed F_3 would reach a maximum value, F_{3max}, at the onset of necking. Therefore, F_2 has a minimum value as shown in the following formula under the formable conditions:

$$F_2 \geqq F_1 - F_{3max} \tag{4}$$

Therefore, we derived the required pad force by deriving the minimum value of F_2. We achieved this by developing and verifying a method to derive the pad force from F_2 as well as methods for F_3 and F_1.

3.5.1 Pad force derivation method using F_2

Fig. 12 shows the surface pressure distribution acting from the pad to the bottom. The pressure on the convex area of bottom was low compared with that on flat area; hence, we assumed that the pad force acts only on the flat area when identifying F_2.

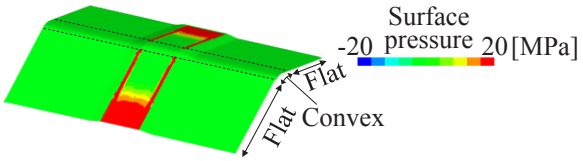

Fig. 12. Surface pressure distribution acting from pad to blank

Therefore, F_2 can be derived from θ, pad force F_p, and friction coefficient μ using the following equation:

$$F_2 = \frac{\mu F_p}{\cos\theta} \tag{5}$$

Fig. 13 shows the results of comparing the theoretical values of F_2 by Eq. (5) and those calculated form FE simulation. The friction force (F_2) in Eq. (5) and the FE simulations. The theoretical and calculated values of F_2 were almost equivalent under all conditions; hence, these results showed that F_p could be predicted from F_2.

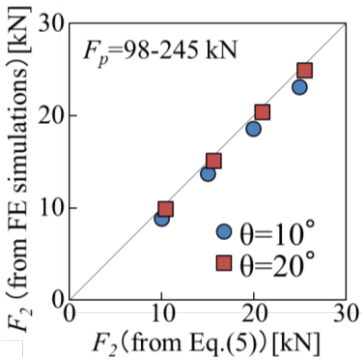

Fig. 13. Results of F_2 verification

3.5.2 Derivation of the maximum value of F_3

We inferred that the maximum value of F_3 (F_{3max}) could be derived through the following equation using the stress σ_{Lmax} at the onset of necking in the plane strain stretching of the material:

$$F_{3max} = \sigma_{Lmax} Wt \tag{6}$$

Since the equivalent stress at the onset of necking in plane strain stretching and in uniaxial tension are identical [3], the following relationship is approximately satisfied for the ultimate tensile strength s_u and the uniform elongation e_u of the material:

$$s_u(1+e_u) = \sigma_{Lmax}\sqrt{1-\frac{2\bar{r}}{1+\bar{r}}\alpha+\alpha^2} \tag{7}$$

with $\alpha=\sigma_T/\sigma_{Lmax}$ where σ_{Lmax} and σ_T are longitudinal and transversal stresses at the onset of necking in plane strain stretching, respectively.

In the plane strain stretching, α can be calculated as $\alpha=\frac{\bar{r}}{1+\bar{r}}$; hence, σ_{Lmax} could be derived from the following equation [3]:

$$\sigma_{Lmax} = s_u(1+e_u)\frac{1+\bar{r}}{\sqrt{1+2\bar{r}}} \tag{8}$$

Fig. 14 shows the results of comparing the value of F_{3max} from Eq. (6), and FE simulation. Eq. (6) gave the values close to those near the necking condition in FE simulations.

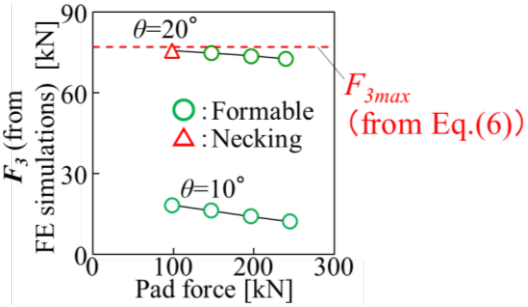

Fig. 14. Results of F_{3max} verification

3.5.3 Derivation of F_1

F_1 is estimated to depend on θ, whereas the shear stress along the edge BC decreases toward the point C, where the value is zero, as shown in Fig. 9. The shear strain at the point C is thought to be smaller than that in the ideal state in Fig. 1 owing to the small material constraint in the longitudinal direction.

Therefore, we used the following equation from the Swift law, where equivalent stress is given as a function of equivalent plastic strain, to calculate the shear stress τ_θ when the wall surface strain γ was assumed to be γ=tanθ:

$$\tau_\theta = \sqrt{\frac{1+\bar{r}}{2(2\bar{r}+1)}} K \left(\varepsilon_0 + \sqrt{\frac{1+\bar{r}}{2(2\bar{r}+1)}} \tan\theta \right)^n \qquad (9)$$

where K, e_0, and n are material parameters [3].

We then assessed the ratio D between τ_θ in Eq. (9) and the shear stress averaged over the edge BC in FE simulations.

Fig. 15 shows the shear stress ratio $D = N\tau_\theta / \sum\tau_i$ for various θ. The values of $\sum\tau_i/N$ in the simulation were smaller than those of τ_θ in Eq. (9). Furthermore, D decreased with decreasing θ. This result was thought to be due to not only the influence of material constraints, but also the fact that the in-plane shear strain was smaller than that of Eq. (9), which is the ideal state, owing to the stroke at the early forming stages being the target of study.

Therefore, it is obvious that these influencing factors must be considered when deriving F_1. These are tasks for future study, but within the scope of our present study, we sought to assess only predictability by verifying whether F_1 in the FE simulations at $\theta > 20°$ could be predicted using a function obtained by fitting to D for θ ranging from 10° to 20°.

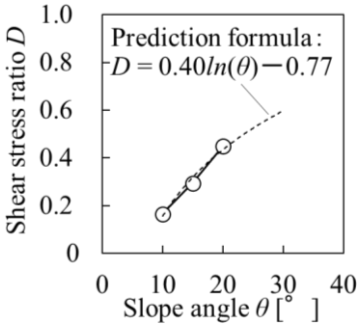

Fig. 15. Shear stress ratio D for various slope angle θ

Fig. 16 shows the results of the validation of the prediction formula. Each value of F_1 was the average under the formable conditions for each θ. The results showed that the prediction formula obtained for θ ranging from 10° to 20° could well predict the values of F_1 in the FE simulations at θ = 25° and 30°.

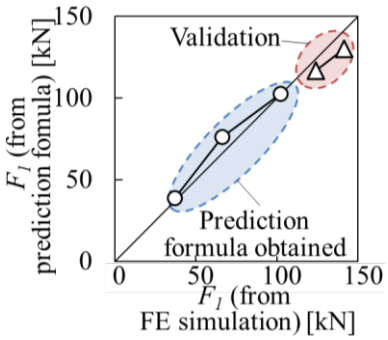

Fig. 16. Verification results of prediction formula for shear stress ratio D

The above study indicates that the required pad force could be derived from the force equilibrium given in Eq. (1). In the future, the material constraints and the shear deformation state of the walls at the early forming stages will be investigated to further discuss the method of deriving F_1. It will also be verified whether the required pad force can be derived based on this theoretical model. Thus, we aim to improve the prediction accuracy of the required pad force.

4 Conclusions

In this study, we focused on the in-plane shear draw-bending, which can produce curved hat channels with high-strength sheet steels, and investigated a method of deriving the minimum pad force required for forming without cracking. The following findings were obtained consequently.

(1) Decreases in pad force increased the plane strain stretching, near the convex bottom, which eventually lead to cracks at the flat end.

(2) For a flat area of bottom in a convex channel, we verified the longitudinal force equilibrium which consists of a force given by in-plane shear of walls, a frictional force given by the pad force for clamping and a resistance against the flow to the convex bottom.

(3) The required pad force could be derived from the force equilibrium at the onset of necking.

References

1. Y. Tanaka, T. Miyagi, M. Ogawa, J. Natori, M. Sugawara, Proceedings of the 69th Japanese Joint Conf. for the Tech. of Plast., JSTP, 247-248 (2018)
2. Y. Tanaka, T. Miyagi, M. Ogawa, J. Natori, M. Sugawara, Proceedings of the 69th Japanese Joint Conf. for the Tech. of Plast., JSTP, 249-250 (2018)
3. T. Kuwabara, J.JILM, **48**, 11, 548-555 (1998)